Atmos. Chem. Phys. Discuss., 10, 10429–10462, 2010
www.atmos-chem-phys-discuss.net/10/10429/2010/

Atmospheric Chemistry and Physics Discussions

This discussion paper is/has been under review for the journal Atmospheric Chemistry and Physics (ACP). Please refer to the corresponding final paper in ACP if available.

Aerosol effects on ice clouds: can the traditional concept of aerosol indirect effects be applied to aerosol-cloud interactions in cirrus clouds?

S. S. Lee and J. E. Penner

Department of Atmospheric, Oceanic, and Space Sciences, University of Michigan, Ann Arbor, MI, USA

Received: 19 January 2010 – Accepted: 16 March 2010 – Published: 21 April 2010

Correspondence to: S. S. Lee (seoungl@umich.edu)

Published by Copernicus Publications on behalf of the European Geosciences Union.

Abstract

Cirrus clouds cover approximately 20–25% of the globe and thus play an important role in the Earth's radiation budget. This indicates that aerosol effects on cirrus clouds can have a substantial impact on the variation of global radiative forcing if the ice-water path (IWP) changes. This study examines the aerosol indirect effect (AIE) through changes in the IWP for a cirrus cloud case. We use a cloud-system resolving model (CSRM) coupled with a double-moment representation of cloud microphysics. Intensified interactions among the cloud ice number concentration (CINC), deposition and dynamics play a critical role in the IWP increases due to aerosol increases. Increased aerosols lead to increased CINC, providing increased surface area for water vapor deposition. The increased deposition causes depositional heating which produces stronger updrafts, and leads to the increased IWP. The conversion of ice crystals to aggregates through autoconversion and accretion plays a negligible role in the IWP responses to aerosols, as the sedimentation of aggregates. The sedimentation of ice crystals plays a more important role in the IWP response to aerosol increases than the sedimentation of aggregates, but, not more important than the interactions among the CINC, deposition and dynamics.

1 Introduction

Aerosols act as cloud condensation nuclei (CCN) and thus affect cloud properties. Increasing aerosol mass and number are known to decrease droplet size and thus increase cloud albedo (first AIE) (Twomey, 1974, 1977). They may also suppress precipitation and, hence, alter cloud mass and lifetime (second AIE) (Albrecht, 1989). An enormous effort has been made to gain an understanding of the effect of aerosols on clouds, since these effects have been considered to be critical for the correct assessment of climate change induced by human activities (Penner et al., 2001).

The aerosol indirect effect was proposed based on observational and modeling stud-

ACPD

10, 10429–10462, 2010

ies of warm stratiform clouds (Twomey, 1977; Albrecht, 1989) and most climate studies have focused on the effect of aerosols on warm stratiform clouds for the prediction of climate change.

Lee et al. (2009) showed that aerosols can lead to significant changes at the top of the atmosphere (TOA) longwave radiation as well as shortwave radiation through their effects on cirrus clouds. Cirrus clouds cover approximately 20–25% of the globe and as much as 70% over the tropics and, thus, can act as one of major modulators of the global radiation budget (Liou, 1986, 2005). Hence, the effect of aerosols on cirrus clouds may have contributed to changes in the global radiation budget and to climate change since industrialization.

Lee et al. (2009) focused on cirrus clouds detrained from deep convective clouds. The radiative properties of these cirrus clouds are mainly determined by ice-crystal formation and growth in deep convective clouds (Houze, 1993). About half of the large-scale cirrus clouds have their origins in the upper layers detrained from deep, precipitating cloud systems (Houze, 1993). The other half of cirrus clouds has their origins in large-scale vertical motions, with velocities much smaller than the vertical velocity in deep convective clouds. Different dynamic intensity (i.e., vertical velocity) is likely to lead to different interactions between microphysics and dynamics by affecting the magnitude of deposition and sublimation. Hence, the properties of cirrus clouds and thus the effects of aerosols on clouds with the weak large-scale motion are likely to be different from those coupled with strong deep convective motion.

In this study, the effect of aerosols on cirrus clouds developing with the vertical velocity associated with large-scale low vertical motion is examined using a CSRM.

ACPD
10, 10429–10462, 2010

2 CSRM

2.1 Dynamics and turbulence

For numerical experiments, the Goddard Cumulus Ensemble (GCE) model (Tao et al., 2003) is used as a three-dimensional nonhydrostatic compressible model. The detailed equations of the dynamical core of the GCE model are described by Tao and Simpson (1993) and Simpson and Tao (1993).

The subgrid-scale turbulence used in the GCE model is based on work by Klemp and Wilhelmson (1978) and Soong and Ogura (1980). In their approach, one prognostic equation is solved for the subgrid-scale kinetic energy, which is then used to specify the eddy coefficients. The effect of condensation on the generation of subgrid-scale kinetic energy is also incorporated into the model.

2.2 Microphysics and radiation

To represent microphysical processes, the GCE model adopts the double-moment bulk representation of Saleeby and Cotton (2004). The size distribution of hydrometeors obeys a generalized gamma distribution:

$$n(D) = \frac{N_t}{\Gamma(\upsilon)} \left(\frac{D}{D_n}\right)^{\nu-1} \frac{1}{D_n} \exp\left(-\frac{D}{D_n}\right) \quad (1)$$

where D is the equivalent spherical diameter (m) (for ice crystals, D is the crystal maximum dimension), $n(D)\,dD$ the number concentration (m^{-3}) of particles in the size range dD and N_t the total number of particles (m^{-3}). Also, ν is the gamma distribution shape parameter (non-dimensional), D_n is the characteristic diameter of the distribution (m), and $\Gamma(\upsilon)$ the complete gamma function of υ.

Full stochastic collection solutions for self-collection among cloud droplets (or cloud liquid) and ice crystals (or cloud ice) and for the collection of cloud droplets and ice crystals by precipitable hydrometeors based on Feingold et al. (1988) are obtained using

ACPD
10, 10429–10462, 2010

realistic collection kernels; there are five classes of precipitable hydrometeors, which are rain, snow, aggregates, graupel, and hail. Hence, this study does not constrain the system to constant or average collection efficiencies. Following Walko et al. (1995), lookup tables are generated and used in each collection process. This enables fast and accurate solutions to the collection equations. In this study, snow is treated as a part of cloud ice or ice crystals, since snow is defined as ice crystals that grow by deposition to larger than 125 μm in the maximum dimension in the bulk representation of Saleeby and Cotton (2004).

The bin representation of collection is adopted for the calculations of hydrometeor sedimentation. Bin sedimentation is simulated by dividing the gamma distribution into discrete bins and then building lookup tables to calculate how much mass and number in a given grid cell falls into each cell beneath a given level in a given time step. 36 bins are used for collection and sedimentation. This is because Feingold et al. (1999) reported that the closest agreement between a full bin-resolving microphysics model in a large eddy simulation (LES) of marine stratocumulus cloud and the bulk microphysics representation was obtained when collection and sedimentation were simulated by emulating a full-bin model with 36 bins.

All the cloud species here have their own terminal velocity. The terminal velocity of each species is expressed as power law relations (See Eq. 7) in Walko et al., 1995). A Lagrangian scheme is used to transport the mixing ratio and number concentration of each species from any given grid cell to a lower height in the vertical column, following Walko et al. (1995).

The parameterizations developed by Chou and Suarez (1999) for shortwave radiation and by Chou and Kouvaris (1991), Chou et al. (1999), and Kratz et al. (1998) for longwave radiation have been implemented in the GCE model. The solar radiation scheme includes absorption due to water vapor, CO_2, O_3, and O_2. Interactions among the gaseous absorption and scattering by clouds, molecules, and the surface are fully taken into account. Reflection and transmission of a cloud layer are computed using the δ-Eddington approximation. Fluxes for a composite of layers are then computed

ACPD
10, 10429–10462, 2010

using the two-stream adding approximation. In computing thermal infrared fluxes, the k-distribution method with temperature and pressure scaling is used to compute the transmission function.

2.3 Ice nucleation

Lohmann and Diehl's (2006) parameterizations, taking into account the dependence of ice nuclei (IN) activation on dust and black carbon (BC) aerosol mass concentration, are used for contact, immersion, and condensation-freezing activation of IN. For contact activation:

$$\frac{dN_{\mathrm{CNT}}}{dt}(\mathrm{m}^{-3}\ \mathrm{s}^{-1}) = m_{io} D_{ap} 4\pi r_{\mathrm{cm}} N_{a,\mathrm{cnt}} \frac{\rho_a n_c^2}{q_c} \tag{2}$$

where $\frac{dN_{\mathrm{CNT}}}{dt}$ is the rate of the production of ice-crystal number concentration via contact freezing, m_{io} (10^{-12} kg) is the original mass of a newly formed ice crystal, D_{ap} ($\mathrm{m}^2\ \mathrm{s}^{-1}$) is the Brownian aerosol diffusivity, r_{cm} (m) is volume-mean droplet radius, $N_{a,\mathrm{cnt}}$ (m^{-3}) is the number concentration of contact nuclei and q_c ($\mathrm{kg\,kg}^{-1}$) and n_c (kg^{-1}) are the mass and number mixing ratio of droplets, respectively. $\rho_a$is the air density. D_{ap} is given by

$$D_{ap} = \frac{kTC_c}{6\pi\eta r_m}$$

where k is the Boltzmann constant, T is the temperature, η is the viscosity of air $\{\eta{=}10^{-5}\ (1.718{+}0.0049(T-T_0) - 1.2\times10^{-5}\ (T-T_0)^2)$ in $\mathrm{kg\,m}^{-1}\ \mathrm{s}^{-1}\}$, r_m is the aerosol mode radius, and C_c is the Cunningham correction factor $[C_c = 1 + 1.26(\frac{\lambda}{r_m})(\frac{p_0}{p})(\frac{T}{T_0})]$. The aerosol mode radius is taken to be 0.2 µm for dust and 0.1 µm for BC. λ is the mean free path length of air ($\lambda = 0.066$ µm at the surface), p_0 and T_0 refer to standard pressure of 101 325 Pa and freezing temperature of 273.15 K. $N_{a,\mathrm{cnt}}$ is obtained from the number concentration of aerosol particles consisting of BC and dust, multiplied by

ACPD
10, 10429–10462, 2010

a temperature dependence of the individual species. This temperature dependence is based on Fig. 1 in Lohmann and Diehl (2006). Here, for dust, the temperature dependence of montmorillonite is adopted (Lohmann and Diehl, 2006). For immersion and condensation-freezing activation:

$$\frac{dN_{\mathrm{IMM}}}{dt}(\mathrm{m}^{-3}\ \mathrm{s}^{-1}) = N_{a,\mathrm{imm}} \exp(T_0 - T)\frac{dT}{dt}\frac{\rho_a q_c}{\rho_w} \quad (3)$$

where $\frac{dN_{\mathrm{IMM}}}{dt}$ is the rate of the production of ice-crystal number concentration via immersion and condensation freezing, T_0 freezing temperature. $N_{a,\mathrm{imm}}$ (m^{-3}) is the number concentration of immersion and condensation nuclei calculated as the number concentration of BC and dust aerosols, multiplied by a temperature dependence for immersion and condensation freezing in Fig. 1 in Lohmann and Diehl (2006). As for contact freezing, the temperature dependence of montmorillonite is adopted for dust. For deposition nucleation, the parameterization of Möhler et al. (2006) is implemented. The rate of production of ice-crystal number concentration via deposition freezing is:

$$\frac{dN_{\mathrm{DEP}}}{dt}(\mathrm{m}^{-3}\ \mathrm{s}^{-1}) = N_{a,\mathrm{dep}}(\exp[a(S_i - S_0)] - 1) \quad (4)$$

where a and S_0 are non-dimensional empirical constants determined by chamber experiments, which are dependent on aerosol properties. Here a and S_0 are set to 4.77 and 1.07, respectively, based on experiments for desert dust. $N_{a,\mathrm{dep}}$ is the number concentration of deposition nuclei (m^{-3}) calculated from predicted total dust mass concentration. Equation (4) is applied at temperatures colder than −40 °C and restricted to $S_0 < S_i < 1.63 + 6.52 \times 10^{-3} \times (T - T_0)$, corresponding to the measured saturation region of Field et al. (2006) where pure deposition nucleation occurs. The parameterization is limited to activating a maximum of 5% of the dust, following the measurements of Field et al. (2006). As indicated by the experiments of Field et al. (2006), Eq. (4) is only valid at temperatures below −40 °C. At temperatures warmer than −40 °C, the parameterizations of Meyer et al. (1992) and DeMott et al. (2003), multiplied by a scaling

ACPD
10, 10429–10462, 2010

factor to consider the dependence of IN activation on dust mass concentration, are used. These parameterizations are applied to grid points with no cloud liquid to ensure only deposition nucleation is calculated. It is limited to activating a maximum of 0.5% of the dust, since Field et al. (2006) found that deposition nucleation did not activate more than 0.5% of the dust at temperatures warmer than −40 °C. Details of these parameterizations can be found in Appendix A.

Secondary production of ice occurs by the Hallet-Mossop process of rime splintering (Hallet and Mossop, 1974) and involves 350 ice splinters emitted for every milligram of rimed liquid at −5.5 °C. The number of splinters per milligram of rimed liquid is linearly interpolated to zero between −3 and −8 °C.

Homogeneous aerosol (haze particle) freezing is assumed to occur instantaneously when a size- and temperature-dependent critical supersaturation with respect to ice for the freezing is exceeded. It is represented by considering the predicted size distribution of unactivated aerosols. A look-up table for the critical supersaturation ratio at which CCN freezes homogeneously is based on the theory proposed by Koop et al. (2000).

2.4 Crystal habit

To account for the variability of crystal type under different environmental conditions, the capacitance and mass-dimensional relations of pristine ice crystals and snow are allowed to vary. Since the model does not keep track of the history of all crystals, a simple diagnostic check of the ambient temperature and saturation conditions at each grid location is performed during each time-step to determine the crystal habit; see Table 1 in Meyers et al. (1997) for the habit diagnosis adopted here. The habit diagnosis impacts the model in several ways. The capacitance is dependent on crystal type (Harrington et al., 1995) and may change the growth characteristics of the crystals. Different types of crystals fall at different speeds which is determined by the power law relation

$$v_t = a_{vt} D^{b_{vt}} \quad (5)$$

ACPD
10, 10429–10462, 2010

where D is the crystal maximum dimension and a_{vt} and b_{vt} are constants for a given crystal habit (see Walko et al. (1997) for details of these constants).

3 Case descriptions

A case of cirrus clouds located at (20° N, 30° W) off the coast of Western Africa is simulated here. A pair of simulations from 06:00 LST (local solar time) on 1 July to 18:00 LST on 1 July in 2002 are performed in which the aerosol concentration is varied from the preindustrial (PI) level to the present-day (PD) level. The simulation with the PD (PI) level is referred to as the high-aerosol (low-aerosol) run, henceforth.

Reanalysis data from the European Centre for Medium-Range Weather Forecasts (ECMWF) provide initial conditions and large-scale forcings. The 6-hourly analyses were applied to the model as a large-scale advection for potential temperature and specific humidity at every time step by interpolation. Temperature and humidity were nudged toward the large-scale fields from the ECMWF using the large-scale advection. The horizontally averaged wind from the GCE model was also nudged toward the interpolated wind field from the ECMWF at every time step with a relaxation time of one hour, following Xu et al. (2002). The model domain is considered to be small compared to large-scale disturbances. Hence, the large-scale advection is approximated to be uniform over the model domain and large-scale terms are defined to be functions of height and time only, following Krueger et al. (1999). Identical observed surface fluxes of heat and moisture were prescribed in both the high- and low-aerosol runs. This method of modeling cloud systems was used for the CSRM comparison study by Xu et al. (2002). The details of the procedure for applying large-scale forcing are described in Donner et al. (1999) and are similar to the method proposed by Grabowski et al. (1996).

Vertical profiles of the initial specific humidity and potential temperature applied to simulations here between 12 and 15 km are shown in Fig. 1; the simulated cloud layer (which will be described later) is located between 12.5 and 14.5 km. The vertical distribution of the time- and area-averaged large-scale forcings of temperature and hu-

ACPD
10, 10429–10462, 2010

midity imposed between 12 and 15 km is depicted in Fig. 2. Initial humidity decreases with height nearly monotonically. Initial potential temperature increases with height with a less stable layer between 13.5 and 14.5 km than above and below these levels as shown in Fig. 1. The large-scale potential-temperature forcing shows two peaks around 12.5 and 14.5 km and the large-scale humidity forcing increases up to around 12.5 km and then decreases to zero around 14 km.

Background aerosol data for the high-aerosol run and the low-aerosol run were provided by the CAM-UMICH model. Aerosol data produced at (20° N, 30° W) from the PD and PI emissions were used for the high-aerosol run and low-aerosol run, respectively. The detailed description of the CAM-UMICH model and aerosol emissions can be found in Wang et al. (2009). The aerosol number concentration is calculated from the mass profiles using the parameters (mode radius, standard deviation, and partitioning among modes) described in Chuang et al. (1997) for sulfate aerosols and Liu et al. (2005) for non-sulfate aerosols (e.g., fossil fuel BC/OM, biomass BC/OM, sea salt, and dust). Here, a bi- or tri-modal log-normal size distribution is assumed for aerosols and the number of aerosols in each size bin of the distribution is determined using these parameters and an assumed aerosol particle density for each species. As for the large-scale advection, the background aerosols are approximated to be uniform over the model domain and defined to be functions of height and time only. The time- and area-averaged vertical distribution of total background aerosol number between 12 and 15 km is shown in Figure 3a. Generally, the aerosol number varies between 15 (10) and 30 (15) cm^{-3} for the high-aerosol (low-aerosol) run.

The aerosol is predicted within clouds and reset to the background value at all levels outside of cloud. Within clouds, aerosols are advected, diffused, and depleted by nucleation of droplets and ice crystals (nucleation scavenging). Initially, the aerosol number is set equal to its background value everywhere. Hence, we focus on the examination of cloud responses to a given aerosol variation in the background since industrialization while considering the effect of cloud-scale processes on aerosols within clouds.

Figure 3b shows the time series of the time- and domain-averaged total background

ACPD
10, 10429–10462, 2010

aerosol number over the layer between 12 and 15 km. Figure 3b indicates that aerosol number does not vary significantly over the simulation period.

The simulations are performed in a 3-D framework. A uniform grid length of 100 m is used in the horizontal domain and the vertical grid length is uniformly 50 m above 10 km. Periodic boundary conditions are used on the horizontal boundaries. The horizontal domain length is set to 12 km in both the east-west and north-south directions. The vertical domain length is 20 km to cover the troposphere and the lower stratosphere.

4 Results

4.1 Cloud properties

Clouds in the high- and low-aerosol runs are formed around 07:00 LST. Figure 4 depicts the temporal evolution of cloud-top and cloud-base height (upper two lines are for cloud-top and lower two lines for cloud-base) from 10 min after the cloud formation to the end of simulation. Figure 4 indicates that cloud depth is ~2 km.

Figure 5 shows the temporal evolution of domain-averaged IWP. Figure 5 shows that the IWP in the high-aerosol run is generally higher than that in the low-aerosol run by ~1–2 g m^{-2} during the time integration. Time- and domain-averaged IWPs are 2.68 (2.11) g m^{-2} for the high (low) aerosol case.

The simulated IWP in the high-aerosol run is compared to observations by the Moderate Resolution Imaging Spectroradiometer (MODIS) to assess the ability of the model to simulate cirrus clouds. The difference between the domain-averaged IWP in the high-aerosol run and MODIS-observed IWP is less than 10% relative to IWP observed by the MODIS. This demonstrates that the IWP is simulated reasonably well.

ACPD
10, 10429–10462, 2010

4.2 Ice-water budget

To elucidate the microphysical processes leading to the increase in IWP with increasing aerosols, the domain-averaged cumulative source (i.e., deposition) and sinks of cloud ice and their differences between the high-aerosol run and low-aerosol run (high aerosol – low aerosol) are obtained. For this, a production equation for cloud ice is integrated over the domain and duration of the simulations. Integrations over the domain and duration of simulation are denoted by < >:

$$< A >= \frac{1}{LxLy} \iiint \rho_a A dx dy dz dt \quad (6)$$

where Lx and Ly are the domain length (12 km), in east-west and north-south directions, respectively, ρ_a is the air density and A represents any of the variables in this study. The budget equation for cloud ice is as follows:

$$< \frac{\partial q_i}{\partial t} >=< Q_{\text{depo}} > - < Q_{\text{subl}} > - < Q_{\text{auto}} > - < Q_{\text{accr}} > \quad (7)$$

Here, q_i is cloud-ice mixing ratio. Q_{depo}, Q_{subl}, Q_{auto}, and Q_{accr} refer to the rates of deposition, sublimation, autoconversion of cloud ice to aggregates, and accretion of cloud ice by aggregates, respectively.

Table 1 shows the budget numbers for Eq. (7) for the high- and low-aerosol runs. The high- and low-aerosol runs (CINC-high fixed) and (CINC-low fixed) will be described in the following sections. The budget numbers show that deposition and sublimation of cloud ice are ∼one to two orders of magnitude larger than autoconversion and accretion. This indicates that the conversion of cloud ice (produced by deposition) to aggregates is highly inefficient in the high- and low-aerosol runs.

Autoconversion and accretion are processes that control the growth of aggregates and sedimentation of aggregates is generally proportional to the size of aggregates. Hence, the small contribution of autoconversion and accretion to IWP implies that cloud-mass (i.e., sum of cloud ice and aggregate) changes due to sedimentation of aggregates are not as significant as those due to deposition and sublimation.

ACPD
10, 10429–10462, 2010

Much larger differences in deposition and sublimation as compared to those in autoconversion and accretion between the high- and low-aerosol runs are simulated here (Table 1). This implies that changes in deposition and sublimation due to aerosol increases play much more important roles in the cloud-mass responses to aerosols than those in the sedimentation of aggregates.

Table 1 shows the domain-averaged cumulative cloud-mass changes due to in-cloud sedimentation of aggregates for the high- and low-aerosol runs; here, the absolute value of the sedimentation-induced mass change is presented. In Table 1, the rates of sedimentation of aggregates and cloud ice are represented by Q_{ased} and Q_{ised}, respectively, and the absolute value of any variable A is represented by $|A|$. The magnitude of deposition is ~one order of magnitude larger than that of cloud-mass changes induced by the sedimentation of aggregates (Table 1). Also, the magnitude of the difference in deposition between the high- and low-aerosol runs is ~two to three orders of magnitude larger than that for mass changes induced by the sedimentation of aggregates (Table 1). Hence, in general, as implied by the budget analysis, the role of the sedimentation of aggregates in the determination of the cloud mass and its response to aerosols is negligible as compared to that of deposition. The role of the sedimentation of cloud ice plays a much more important role in this determination and response than that of the sedimentation of aggregates as shown in Table 1. However, the role of deposition is still much more important than that of the sedimentation of cloud ice. The domain-averaged cumulative cloud-mass changes due to in-cloud sedimentation of cloud ice is ~13 and 16% of the domain-averaged cumulative deposition in the high-aerosol run and the low-aerosol run, respectively. Also, the difference in the sedimentation of cloud ice between the high- and low-aerosol runs is ~3% of that in deposition.

ACPD
10, 10429–10462, 2010

4.3 Factors controlling deposition

The mass changes of ice crystals from the diffusion of vapor, integrated over the size distribution, is as follows:

$$\frac{d\overline{m}}{dt} = N_i 2\pi\psi F_{Re} S \rho_{vsh} \tag{8}$$

where N_i is CINC, ψ the vapor diffusivity, and $\rho_{\text{vsh}}$the saturation water vapor mixing ratio over ice. S is the supersaturation, given by $\left(\frac{\rho_{va}}{\rho_{vsh}} - 1\right)$ where ρ_{va} is water vapor mixing ratio. F_{Re} is the integrated product of the ventilation coefficient, the crystal shape factor and the maximum dimension which is given by

$$F_{Re} = \int_0^\infty S_h D f_{Re} f_{\text{gam}}(D) dD \tag{9}$$

where D is the crystal maximum dimension, S the crystal shape factor that is defined as $S_h = \frac{C}{D}$ with C the crystal capacitance, f_{Re} the ventilation coefficient, and $f_{\text{gam}}(D)$ the gamma distribution function, given by Eq. (1). f_{Re} is given by $\left[1.0 + 0.229\left(\frac{v_t D}{V_k}\right)^{0.5}\right]\eta$ where v_t is the terminal velocity and V_k the kinematic viscosity of air and $\eta$the shape parameter (Cotton et al., 1982).

Among the variables associated with the depositional growth of cloud ice in Eq. (8), differences in the supersaturation and CINC contribute most to the differences in deposition between the high- and low-aerosol runs. Percentage differences in the other variables are found to be ~two orders of magnitude smaller than those in supersaturation and CINC throughout the simulations. Figure 6a shows the time series of CINC and Fig. 6b the time series of supersaturation. Figure 6b indicates that supersaturation is generally larger at low aerosol than at high aerosol. However, the deposition rate is generally higher, leading to larger cumulative deposition at high aerosol than at low

aerosol (Table 1). This is ascribed to the larger CINC (as shown in Fig. 6a) providing a larger surface area for water-vapor deposition at high aerosol compared to that at low aerosol. The effects of the CINC increase on the surface area of cloud ice and thus deposition compete with the effects of the supersaturation decrease on the deposition with increasing aerosols. This leads to a smaller deposition difference than the differences in CINC and supersaturation. The effects of the increased surface area for deposition outweigh the effects of decreased supersaturation, leading to the increase in vapor deposition in the high aerosol run.

Increased deposition provides more depositional heating, and, thereby, intensifies updrafts as shown in Fig. 6c which depicts the time series of domain-averaged updraft mass fluxes. Increased updrafts in turn increase deposition, establishing a positive feedback between updrafts and deposition. Therefore, the ice crystal number concentration provides a larger surface area for deposition and plays a critical role in increasing both deposition and updrafts. The interactions among CINC, deposition and dynamics (i.e., updrafts) play the most important role in the determination of the differences in deposition and thereby the IWP response to aerosols between the high- and low-aerosol runs.

4.4 Runs with different CINC for deposition

To isolate the role of the impacts of CINC (i.e., the surface area of ice crystals) on deposition in making IWP differences, the high- and low-aerosol runs are repeated with identical CINC only for deposition but not for the other processes including sublimation. This simulates the IWP differences in the absence of the impacts of the surface area of ice crystals on deposition. The comparison of these simulations to simulations described in previous sections (i.e., the high- and low-aerosol runs) enables an assessment of the contribution of aerosol and thus CINC impacts on deposition to the IWP differences.

Two pairs of additional simulations, each of which is composed of the high- and low-aerosol runs, are performed. Each pair of simulations adopts the identical CINC only

ACPD
10, 10429–10462, 2010

for deposition; N_i in Eq. (8) is fixed at a constant value and forced to be the same for the high- and low-aerosol runs, though predicted N_i is allowed to be used in the other processes. The first pair of simulations is referred to as the high-aerosol run (CINC-high fixed) and low-aerosol run (CINC-high fixed) in Table 1. These CINC-high fixed runs adopt the averaged CINC in the high-aerosol run, which is 38 l^{-1}, as a fixed value only for deposition. The second pair of simulations adopt the averaged CINC in the low-aerosol run, which is 21 l^{-1}, as a fixed value only for deposition and are referred to as the high-aerosol run (CINC-low fixed) and the low-aerosol run (CINC-low fixed) in Table 1.

The budget numbers of Eq. (7) for these additional simulations are shown in Table 1. The time- and domain-averaged IWPs in the high-aerosol run (CINC-high fixed) and low-aerosol run (CINC-high fixed) are 2.62 and 2.58 g m^{-2}. The IWP in the low-aerosol run (CINC-high fixed) increases significantly as compared to the IWP in the low-aerosol run, resulting in much smaller differences in IWP between the high- and low-aerosol runs (CINC-high fixed) than those between the high- and low-aerosol runs. This is mainly due to larger CINC in the low-aerosol run (CINC-high fixed) than average CINC in the low-aerosol run, leading to increased deposition as compared to that in the low-aerosol run (Table 1).

The IWP differences between the high-aerosol run (CINC-low fixed) and low-aerosol run (CINC-low fixed) are also much smaller as compared to those in the high- and low-aerosol runs (Table 1). IWPs in the high-aerosol run (CINC-low fixed) and low-aerosol run (CINC-low fixed) are 2.13 and 2.06 g m^{-2}, respectively. IWP in the high-aerosol run (CINC-low fixed) decreases significantly as compared to IWP in the high-aerosol run, resulting in the small differences in IWP between the high-aerosol run (CINC-low fixed) and low-aerosol run (CINC-low fixed) (Table 1). This is mainly due to smaller CINC in the high-aerosol run (CINC-low fixed) than the average CINC in the high-aerosol run, leading to less deposition than in the high-aerosol run (Table 1).

These additional simulations indicate that the IWP responses to aerosols can be nearly the same for the high- and low-aerosol runs only by making the CINC for de-

ACPD
10, 10429–10462, 2010

position identical. This demonstrates the crucial role of CINC impacts on deposition in the IWP responses to aerosols. This also demonstrates that the impacts of aerosols and thus CINC on the other processes such as the sedimentation of ice crystals and aggregates and the conversion of ice crystals to aggregates do not play an important role in the IWP response to aerosols.

4.5 Nucleation

Figure 7 shows the vertical distribution of the in-cloud averaged nucleation rate for each of the high- and low-aerosol runs. The homogeneous freezing of haze particles dominates over the heterogeneous nucleation of ice particles for the production of CINC; the production of CINC through the homogeneous freezing of haze particles is ∼one order of magnitude larger than that through the heterogeneous nucleation of ice particles. Also, the difference in the homogeneous freezing between the high- and low-aerosol runs is ∼one order of magnitude larger than that in the heterogeneous nucleation of ice particles. Haze particles are unactivated droplets which formed on CCN. Hence, the number of haze particles and thus their homogeneous freezing are associated with CCN but not with IN. This indicates that the CINC and its response to aerosols are controlled by CCN but not by IN. To confirm this, simulations are repeated with no variation of aerosols acting as CCN (fixed at the PI level) but with the variation of aerosols (from their PI level to PD level) acting as IN between the high- and low-aerosol runs. These simulations show that ∼2% of the variation in deposition and ∼5% of the variation in IWP as compared to those in the standard high- and low-aerosol runs. However, another set of repeated simulations only with CCN variation (with no variation of IN, which was fixed at the PI level) shows 98% of the variation in deposition and 94% of the variation in IWP as compared to those in the standard high- and low-aerosol runs. Hence, these repeated simulations demonstrate that the results here are strongly sensitive to the CCN variation and that their dependence on IN variation is negligible.

ACPD
10, 10429–10462, 2010

4.6 Radiation budget

Upward shortwave and longwave fluxes at the top of the atmosphere (TOA) are presented in Table 2. In Table 2, SW and LW represent upward shortwave and longwave fluxes.

The low-aerosol run has a smaller TOA upward SW (here, TOA is at the level of 0.01 hPa) than the high-aerosol run; more SW is reflected in the high-aerosol run than in the low-aerosol run by 15.4 $W m^{-2}$, which is associated with the larger IWP in the high-aerosol run than in the low-aerosol run.

Increased cloud mass causes more LW emitted from the surface to be absorbed by clouds at high aerosol, leading to smaller outgoing LW at the TOA in the high-aerosol run than in the low-aerosol run (Table 2). Those changes in LW offset changes in SW. 35% of the increase of the reflected solar radiation due to aerosol increases is offset by the decrease of the outgoing longwave radiation. This offset is much larger than the offset in stratocumulus clouds. For example, Lee et al. (2009) showed that, for the transition from the continental aerosols to maritime aerosols which involves a 10-fold decrease in aerosol number, only less than 3% of increase in the reflection of solar radiation is offset by the decrease in the outgoing longwave radiation in stratocumulus clouds.

It is interesting that the change in LW radiation is smaller than the change in SW radiation for these simulations. Normally, if changes in IWP are not considered, the change in LW radiation dominates that of SW radiation for cirrus clouds perturbed by aerosol concentration (Penner et al., 2009). Here, the increase of IWP has actually reversed this impact.

5 Summary and conclusion

Aerosol-cloud interactions in cirrus clouds developing with the large-scale low vertical motion off the coast of Western Africa in the summer in 2002 were simulated using

ACPD
10, 10429–10462, 2010

a CSRM coupled with a double-moment microphysics. Present-day and preindustrial aerosols were prescribed to examine aerosol effects on IWP.

Simulations showed that increasing aerosols increased IWP. The conversion of ice crystals to aggregates through autoconversion and accretion played a negligible role in the IWP response to aerosols, as did the sedimentation of aggregates. Instead, it was found that feedbacks among CINC, deposition and dynamics played the most important role in the increased IWP at high aerosol; the increased CINC offsets the decreased supersaturation causing an increase in the vapor deposition with the increased aerosols. The role of the sedimentation of ice crystals plays a much more important role in the IWP response than that of the sedimentation of aggregates, though the change in the sedimentation of ice crystals accounted for high and low aerosols is ~two times smaller than the feedbacks among CINC, deposition and dynamics.

The homogeneous freezing of haze particles was most important for the determination of the CINC and its variation with the aerosol concentration. Heterogeneous nucleation processes played a negligible role in the determination of CINC.

The traditional understanding of aerosol-cloud interactions proposed by Albrecht (1989) is based on the observation of warm stratocumulus clouds. It indicates that the response of the liquid-water path (LWP) to aerosol changes is controlled by the conversion of cloud liquid to rain and sedimentation of rain. Cloud ice (or ice crystal) and aggregates in ice clouds above the level of homogeneous freezing (where liquid hydrometeors are absent) is equivalent to cloud liquid (or cloud droplets) and rain, respectively, in warm clouds. This is because cloud ice and cloud liquid both are considered to form from nucleation while rain and aggregates both are considered to form from autoconversion. Adopting this equivalence, it can be said that the traditional understanding of aerosol-cloud interactions is not applicable to the ice clouds simulated here due to the negligible role of the conversion of ice crystals to aggregates and the sedimentation of aggregates in the effect of aerosols on IWP.

The effect of LW radiation changes caused by increasing aerosols on the ice clouds simulated here compensated for ~35% of the increased outgoing SW radiation. Thus,

the increase in IWP and CINC in cirrus clouds with increasing aerosols can enhance the so-called infrared warming effect of these clouds, though the global impact of this effect will depend on the relationship between the distribution of aerosols and synoptic motions in the upper troposphere, a matter which this study was not able to consider.

The growth of ice crystals to precipitable hydrometeors through autoconversion and accretion is more efficient when liquid-phase particles are rimed onto these crystals than when only ice particles are involved in autoconversion and accretion. This is because the collection efficiencies are higher for collisions between liquid- and solid-phase particles than those between solid-phase particles. This contributes to the very low conversion efficiency (i.e., the ratio between the conversion of cloud ice to aggregates and deposition) and sedimentation, leading to a less important role for this conversion and sedimentation in the response of cloud mass to aerosols than that of deposition in this study.

The coarse spatial resolutions employed in climate models are not able to resolve the interactions among CINC, deposition, and updrafts in the cloud layer, which play important roles in aerosol effects on IWP in cirrus clouds here. It is necessary to develop parameterizations that are able to consider the effects of these interactions on the IWP variation with aerosols. Parameterizations for the representation of the IWP variation with aerosols simply relying on changes in autoconversion and sedimentation with varying aerosols with no consideration of feedbacks between microphysics and dynamics in climate models can be misleading. This can contribute to a large uncertainty in the estimation of radiative forcing associated with aerosol indirect effects, considering the significant coverage of cirrus clouds. Also, most of climate models and some of CSRMs have adopted saturation adjustment schemes which are not able to predict supersaturation and to thereby consider the effects of changes in the surface area of cloud particles for the calculation of deposition. Hence, using a saturation adjustment scheme prevents the simulation of the changing competition between supersaturation and the surface area of cloud particles with increasing aerosols. Thus, this prevents the simulation of varying interactions among CINC, deposition, and dy-

ACPD
10, 10429–10462, 2010

namics with aerosols, which can lead to incorrect assessments of aerosol effects on cirrus clouds. Therefore, microphysics parameterizations, able to predict particle mass and number, and thereby, surface area, coupled with a prediction of supersaturation, need to be implemented into climate models for a correct assessment of aerosol effects on cirrus clouds.

The generalization of the results reported here requires further investigation. The set of simulations examined here are too limited to form a generalized basis for determining the effects of aerosol on cirrus clouds and, thus, their parameterizations for large-scale or climate models. More case studies of cirrus clouds developing under various environmental conditions are needed to establish the generalization of the results reported here.

Appendix A

Deposition nucleation at temperatures warmer than −40 °C

At temperatures between −30 and −40 °C and between −5 and −30 °C, DeMott et al. (2003) and Meyers et al.'s (1992) parameterizations, multiplied by a scaling factor, are used for deposition nucleation, respectively. For temperatures between −30 and −0 °C:

$$N_{\mathrm{IN}}(\mathrm{m}^{-3}) = 1000(\exp[12.96(S_i - 1.1)])^{0.3} \times \Psi \quad \text{(A1)}$$

Here, N_{IN} is ice-crystal number concentration, S_i the saturation ratio with respect to ice and Ψ a scaling factor to take into account the dependence of IN activation on dust mass. Ψ is $\frac{DU_{2.5}}{DU^{*}_{2.5}}$, where $DU_{2.5}$ is mass concentration of dust particles with diameter less than 2.5 µm and $DU^{*}_{2.5}$ is a reference dust mass concentration. $DU^{*}_{2.5}$ is set at 0.11 µg m^{-3} based on dust data from the Mount Werner project used to derive Eq. (A1) (DeMott et al., 2003). Hence, Eq. (A1) computes N_{IN} based on variation of dust mass

ACPD
10, 10429–10462, 2010

relative to dust mass observed at the Mount Werner project. It was observed that IN concentrations were almost linear with the concentrations of large aerosol particles (Berezinskiy et al., 1986; Georgii and Kleinjung, 1967), supporting the assumption that N_{IN} is proportional to $DU_{2.5}$. For temperatures between −5 and −30 °C, the same scaling factor as used in Eq. (A1) is applied to the parameterization of Meyers et al. (1992) as follows, since dust mass data are not available in Meyers et al. (1992):

$$N_{IN}(m^{-3}) = 63\exp[12.96(S_i - 1) - 0.639] \times \Psi \quad \text{(A2)}$$

Acknowledgements. The authors wish to thank Derek Posselt for providing the GCE coupled with the double-moment microphysics used here and for valuable discussions. This paper was prepared under US Department of Energy ARM program (DE FG02 97 ER62370).

References

Albrecht, B. A.: Aerosols, cloud microphysics, and fractional cloudiness, Science, 245, 1227–1230, 1989.

Berezinskiy, N. A., Stepanov, G. V., and Khorguani, V. G.: Altitude variation of relative ice-forming activity of natural aerosol, S. Meterol. Hydr., 12, 86–89, 1986.

Chou, M.-D. and Suarez, M. J.: A shortwave radiation parameterization for atmospheric studies, 15, NASA/TM-104606, 40 pp., 1999.

Chou, M.-D., Ridgway, W., and Yan, M.-H.: Parameterizations for water vapor IR radiative transfer in both the middle and lower atmospheres, J. Atmos. Sci., 52, 1159–1167, 1999.

Chuang, C. C., Penner, J. E., Taylor, K. E., Grossman, A. S., and Walton, J. J.: An assessment of the radiative effects of anthropogenic sulfate, J. Geophys. Res., 102, 3761–3778, 1997.

Cotton, W. R., Stephens, M. A., Nehrkorn, T., and Tripoli, G. J.: The Colorado State University three-dimensional cloud/mesoscale model. Part II: An ice phase parameterization, J. Rech. Atmos., 16, 295–319, 1982.

DeMott, P. J., Cziczo, D. J., Prenni, A. J., Murphy, D. M., Kreidenweis, S. M., Thomson, D. S., Borys, R., and Rogers, D. C.: Measurements of the concentration and composition of nuclei for cirrus formation, P. Natl. Acad. Sci. USA, 100(25), 14655–14660, 2003.

Donner, L. J., Seman, C. J., and Hemler, R. S., Three-dimensional cloud-system modeling of GATE convection, J. Atmos. Sci., 56, 1885–1912, 1999.

Feingold, G., Tzivion, S., and Levin, Z.: Evolution of raindrop spectra. Part I: Solution to the stochastic collection/breakup equation using the method of moments, J. Atmos. Sci., 45, 3387–3399, 1988.

Feingold, G., Cotton, W., Kreidenweis, S., and Davis, J.: The impact of giant cloud condensation nuclei on drizzle formation in stratocumulus: Implications for cloud radiative properties, J. Atmos. Sci., 56, 4100–4117, 1999.

Field, P. R., Möhler, O., Connolly, P., Krämer, M., Cotton, R., Heymsfield, A. J., Saathoff, H., and Schnaiter, M.: Some ice nucleation characteristics of Asian and Saharan desert dust, Atmos. Chem. Phys., 6, 2991–3006, 2006, http://www.atmos-chem-phys.net/6/2991/2006/.

Grabowski, W. W., Wu, X., and Moncrieff, M. W.: Cloud resolving modeling of tropical cloud systems during phase III of GATE. Part I: Two-Dimensional Experiments, J. Atmos. Sci., 53, 3684–3709, 1996.

Georgii, H. W. and Kleinjung, E.: Relations between the chemical composition of atmospheric aerosol particles and the concentration of natural ice nuclei, J. Rech. Atmos., 3, 145–146, 1967.

Hallett, J. and Mossop, S. C.: Production of secondary ice particles during the riming process, Nature, 249, 26–28, 1974.

Harrington, J. Y., Michael, P. M., Walko, R. L., and Cotton, R. C.: Parameterization of ice crystal conversion processes due to vapor deposition for mesoscale models using double-moment basis functions. Part I: Basic formulation and parcel model results, J. Atmos. Sci., 52, 4344–4366, 1995.

Houze, R. A.: Cloud dynamics, Academic Press, 573 pp., 1993.

Klemp, J. B. and Wilhelmson, R.: The simulation of three-dimensional convective storm dynamics, J. Atmos. Sci., 35, 1070–1096, 1978.

Koop, T., Luo, B. P., Tsias, A., and Peter, T.: Water activity as the determinant for homogeneous ice nucleation in aqueous solutions, Nature, 406, 611–614, 2000.

Kratz, D. P., Chou, M.-D., Yan, M.-H., and Ho, C.-H.: Minor trace gas radiative forcing calculations using the k-distribution method with one-parameter scaling, J. Geophy. Res., 103, 31647–31656, 1998.

Krueger, S. K., Cederwall, R. T., Xie, S. C., and Yio, J. J.: GCSS Working Group 4 Model Intercomparison-procedures for Case 3: Summer 1997 ARM SCM IOP. Draft manuscript obtainable from http://www.arm.gov/docs/scm/scmic3, 1999.

Lee, S. S., Donner, L. J., and Phillips, V. T. J.: Sensitivity of aerosol and cloud effects on radiation to cloud types: comparison between deep convective clouds and warm stratiform clouds over one-day period, Atmos. Chem. Phys., 9, 2555–2575, 2009, http://www.atmos-chem-phys.net/9/2555/2009/.

Liou, K. N.: Cirrus clouds and climate in McGraw-Hill Yearbook of Science and Technology, 432 pp., 2005.

Liou, K. N.: Influence of cirrus clouds on weather and climate processes: A global perspective, Mon. Weather Rev., 114, 1167–1199, 1986.

Liu, X., Penner, J. E., and Herzog, M.: Global modeling of aerosol dynamics: Model description, evaluation, and interactions between sulfate and nonsulfate aerosols, J. Geophys. Res., 110, D18206, doi:10.1029/2004JD005674, 2005.

Lohmann, U. and Diehl, K.:Sensitivity studies of the importance of dust ice nuclei for the indirect aerosol effect on stratiform mixed-phase clouds, J. Atmos. Sci., 63, 968–982, 2006.

Meyers, M. P., DeMott, P. J., and Cotton, W. R.: New primary ice-nulceation parameterization in an explicit cloud model, J. Appl. Meteor., 31, 708–720, 1992.

Meyers, M. P., Walko, R. L., Harrington, J. Y., and Cotton, W. R.: New RAMS cloud microphysics parameterization. Part II: The two-moment scheme, Atmos. Res., 45, 3–39, 1997.

Möhler, O., Field, P. R., Connolly, P., Benz, S., Saathoff, H., Schnaiter, M., Wagner, R., Cotton, R., Krämer, M., Mangold, A., and Heymsfield, A. J.: Efficiency of the deposition mode ice nucleation on mineral dust particles, Atmos. Chem. Phys., 6, 3007–3021, 2006, http://www.atmos-chem-phys.net/6/3007/2006/.

Penner, J. E., Chen, Y., Wang, M., and Liu, X.: Possible influence of anthropogenic aerosols on cirrus clouds and anthropogenic forcing, Atmos. Chem. Phys., 9, 879–896, 2009, http://www.atmos-chem-phys.net/9/879/2009/.

Penner, J. E., Andreae, M., Annegarn, H., Barrie, L., Feichter, J., Hegg, D., Jayaraman, A., Leaitch, R., Murphy, D., Nganga, J., and Pitari, G.: Aerosols, their Direct and Indirect Effects, in: Climate Change 2001: The Scientific Basis, edited by: Houghton, J. T., Ding, Y., Griggs, D. J., Noguer, M., Van der Linden, P. J., Dai, X., Maskell, K., and Johnson, C. A., Report to Intergovernmental Panel on Climate Change from the Scientific Assessment Working Group (WGI), Cambridge University Press, 289–416, 2001.

Saleeby, S. M. and Cotton, W. R.: A large-droplet mode and prognostic number concentration of cloud droplets in the Colorado state university regional atmospheric modeling system (RAMS). Part I: Module description and supercell test simulations, J. Appl. Meteor., 43, 182–

195, 2004.
Simpson, J. and Tao, W.-K.: The Goddard Cumulus Ensemble model. Part II: Applications for studying cloud precipitating processes and for NASA TRMM, Terr. Atmos. Ocean. Sci., 4, 73–116, 1993.
Soong, S.-T. and Ogura, Y.: Response of trade wind cumuli to large-scale processes, J. Atmos. Sci., 37, 2035–2050, 1980.
Tao, W.-K., Simpson, J., and Baker, J., et al.: Microphysics, radiation and surface processes in the Goddard Cumulus Ensemble (GCE) model, Meteor. Atmos. Phys., 82, 97–137,2003.
Tao, W.-K. and Simpson, J.: The Goddard Cumulus Ensemble model. Part I: Model description, Terr. Atmos. Ocean. Sci., 4, 19–54, 1993.
Twomey, S.: The influence of pollution on the shortwave albedo of clouds, J. Atmos. Sci., 34, 1149–1152, 1977.
Twomey, S.: Pollution and the Plantetary Albedo, Atmos. Environ., 8, 1251–1256, 1974.
Walko, R. L., Cotton, W. R., Meyers, M. P., and J. Y. Harrington, J. Y.: New RAMS cloud microphysics parameterization: Part I. The single-moment scheme, Atmos. Res., 38, 29–62, 1995.
Wang, M., Penner, J. E., and Liu, X.: Coupled IMPACT aerosol and NCAR CAM3 model: Evaluation of predicted aerosol number and size distribution, J. Geophys. Res., 114, D06302, doi:10.1029/2008JD010459, 2009.
Xu, K.-M., Cederwall, R. T., Donner, L. J., et al.: An intercomparison of cloud-resolving models with the Atmospheric Radiation Measurement summer 1997 Intensive Observation Period data, Q. J. Roy. Meteor. Soc., 128, 593–624, 2002.

Table 1. Domain-averaged budget terms of cloud ice.

	High-aerosol	High-aerosol (CINC-high fixed)	High-aerosol (CINC-low fixed)	Low-aerosol	Low-aerosol (CINC-high fixed)	Low-aerosol (CINC-low fixed)	High minus Low	High minus Low (CINC-high fixed)	High minus Low (CINC-low fixed)
IWP ($g\,m^{-2}$)	2.68	2.62	2.13	2.11	2.58	2.06	0.57	0.04	0.07
$< Q_{depo} >$ Deposition (μm)	5.42	5.39	4.68	4.66	5.31	4.58	0.76	0.08	0.10
$< Q_{subl} >$ Sublimation (μm)	1.06	1.02	0.48	0.46	1.01	0.44	0.60	0.01	0.04
$< Q_{auto} >$ Autoconversion of cloud ice to aggregates + $< Q_{accr} >$ Accretion of cloud ice by aggregates (μm)	0.021	0.020	0.015	0.023	0.028	0.022	−0.002	−0.008	−0.007
$< \lvert Q_{ased} \rvert >$ Sedimentation of aggregates above the cloud base (μm)	0.050	0.050	0.047	0.051	0.053	0.050	−0.001	−0.003	−0.003
$< \lvert Q_{ised} \rvert >$ Sedimentation of cloud ice above the cloud base (μm)	0.71	0.71	0.65	0.73	0.74	0.70	−0.02	−0.03	−0.05
$(< Q_{auto} > + < Q_{accr} >) / < Q_{depo} >$; $\lvert \Delta(< Q_{auto} > + < Q_{accr} >) \rvert / \lvert \Delta < Q_{depo} > \rvert$ for "High minus Low"	0.004	0.004	0.003	0.005	0.005	0.005	0.003	0.100	0.070
$< \lvert Q_{ased} \rvert > / < Q_{depo} >$; $\lvert \Delta < \lvert Q_{ased} \rvert > \rvert / \lvert \Delta < Q_{depo} > \rvert$ for "High minus Low"	0.009	0.009	0.010	0.011	0.010	0.011	0.001	0.038	0.030
$< \lvert Q_{ised} \rvert > / < Q_{depo} >$; $\lvert \Delta < \lvert Q_{ised} \rvert > \rvert / \lvert \Delta < Q_{depo} > \rvert$ for "High minus Low"	0.13	0.13	0.14	0.16	0.14	0.15	0.03	0.38	0.50

ACPD
10, 10429–10462, 2010

Table 2. Time- and area-averaged upward shortwave flux (SW) and longwave flux (LW) at the top of the atmosphere (TOA).

Time- and area-averaged upward shortwave and longwave fluxes at the top of the model (W m^{-2})		
	TOA	
	CONTROL	
	SW	LW
Low aerosol	231.1	497.7
High aerosol	246.5	492.2
Difference (high – low)	15.4	–5.5

ACPD
10, 10429–10462, 2010

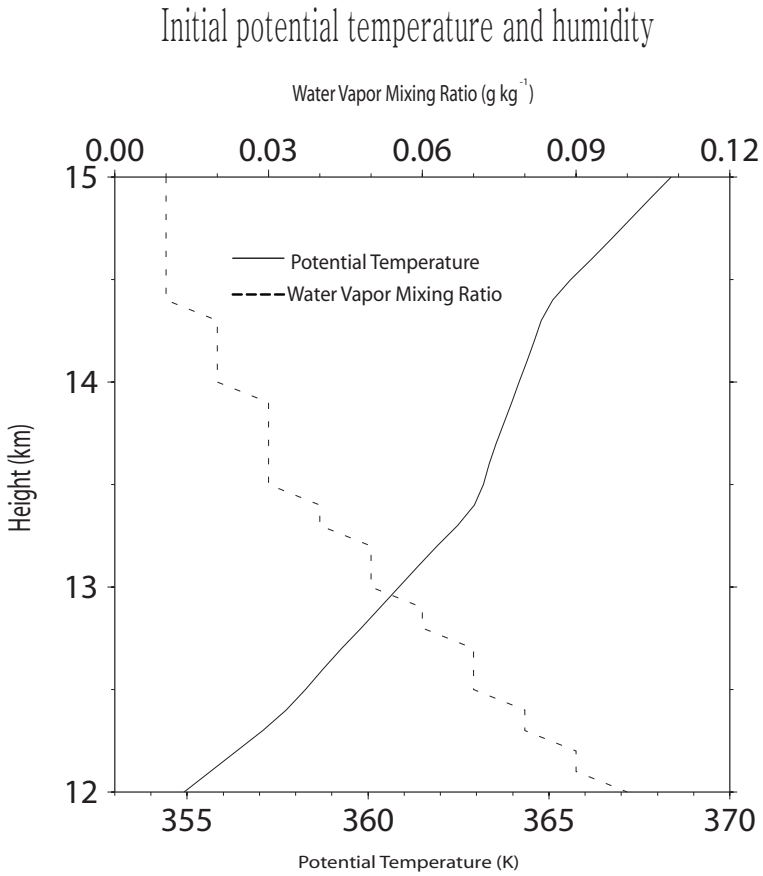

Fig. 1. Vertical profiles of initial potential temperature and water vapor mixing ratio.

ACPD
10, 10429–10462, 2010

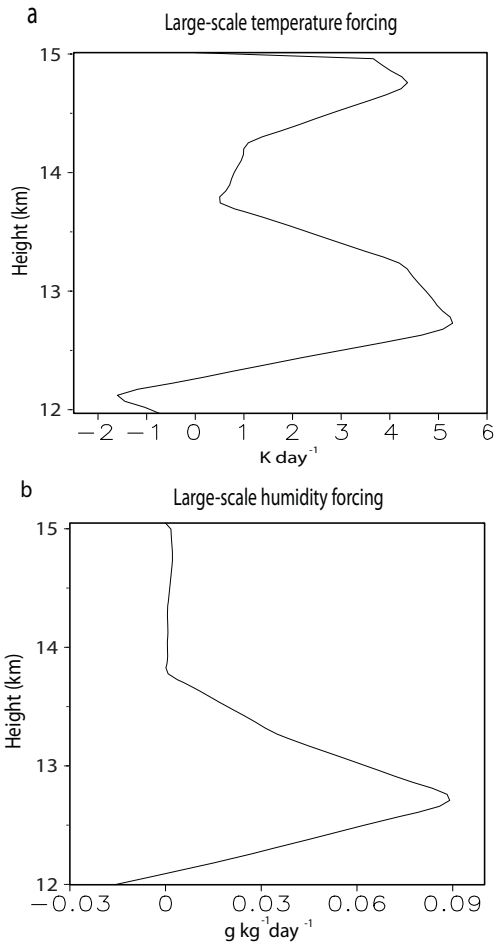

Fig. 2. Vertical distribution of the time- and area-averaged **(a)** potential temperature large-scale forcing and **(b)** humidity large-scale forcing.

ACPD
10, 10429–10462, 2010

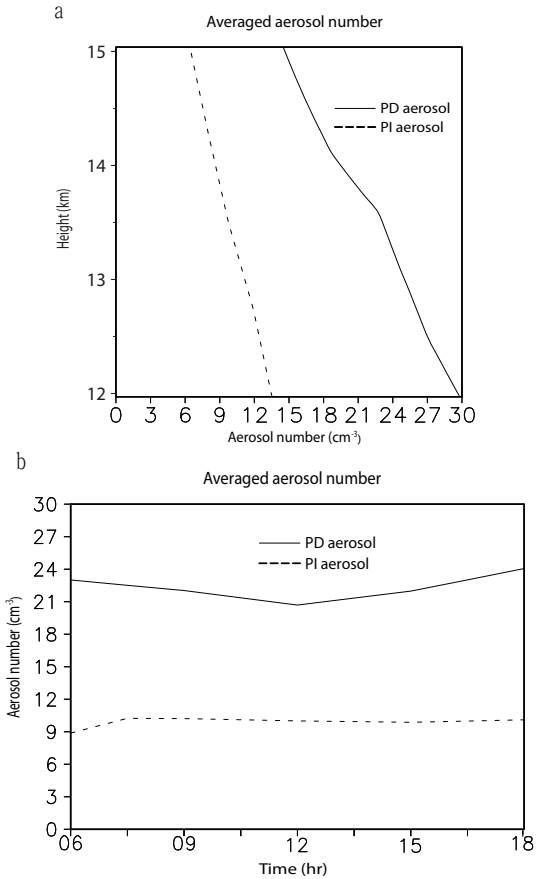

Fig. 3. **(a)** Vertical distribution of the time- and area-averaged background aerosol number concentration and **(b)** the time series of background aerosol number concentration averaged over the layer between 12 and 15 km.

ACPD
10, 10429–10462, 2010

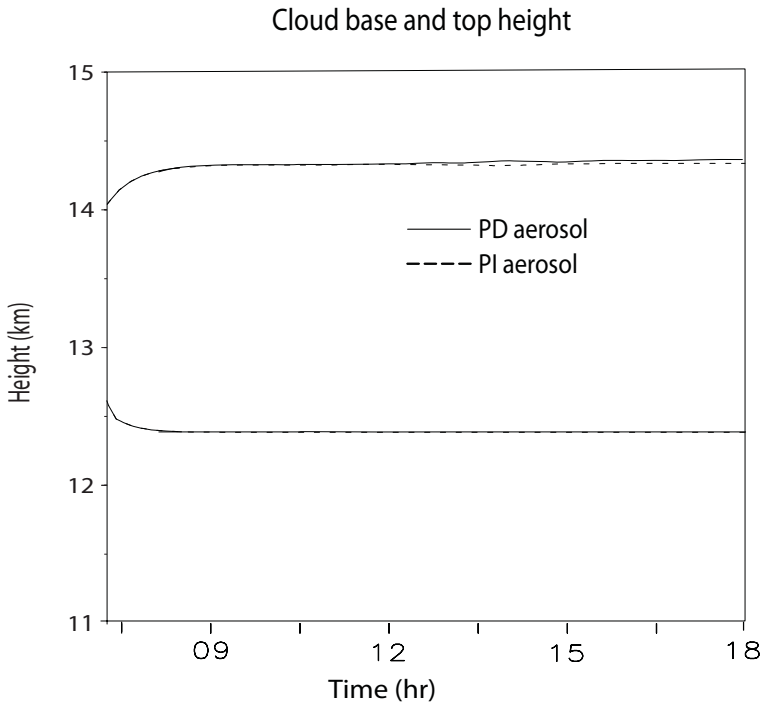

Fig. 4. Time series of cloud-top and cloud-base height. The upper (lower) two lines represent cloud-top (cloud-base) height.

ACPD
10, 10429–10462, 2010

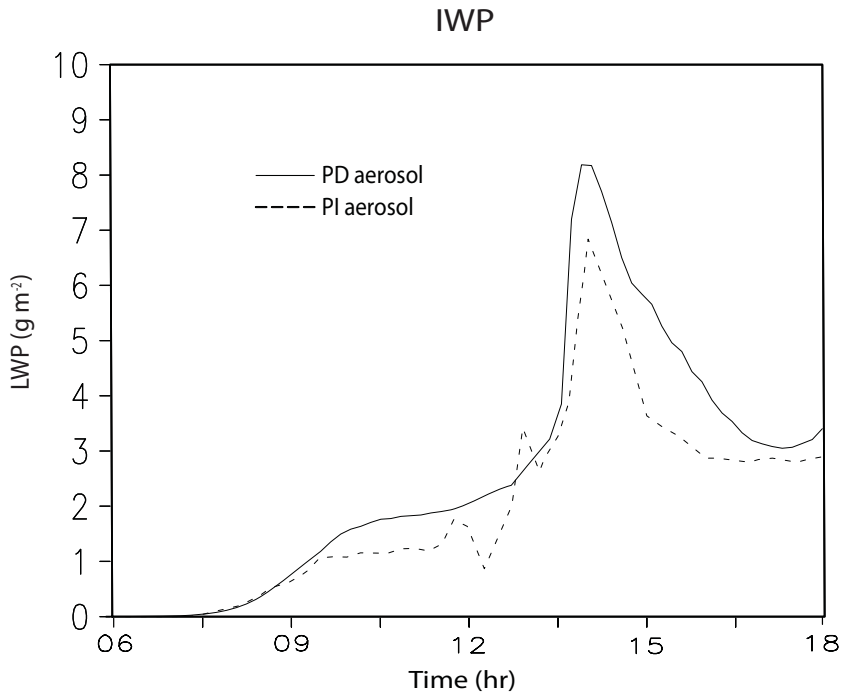

Fig. 5. Time series of the domain-averaged IWP.

ACPD
10, 10429–10462, 2010

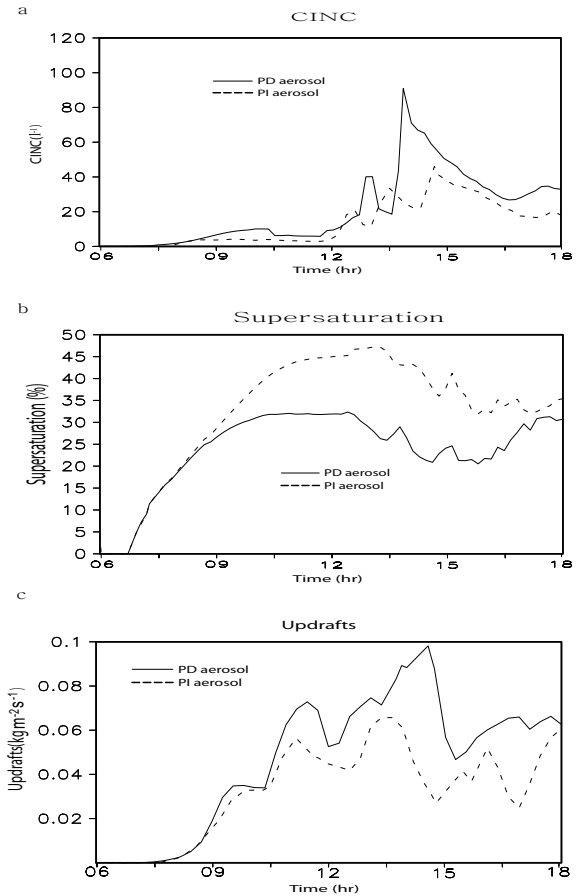

Fig. 6. Time series of conditionally averaged **(a)** CINC and **(b)** supersaturation over areas where deposition rate is positive and **(c)** the time series of the domain-averaged updrafts.

ACPD
10, 10429–10462, 2010

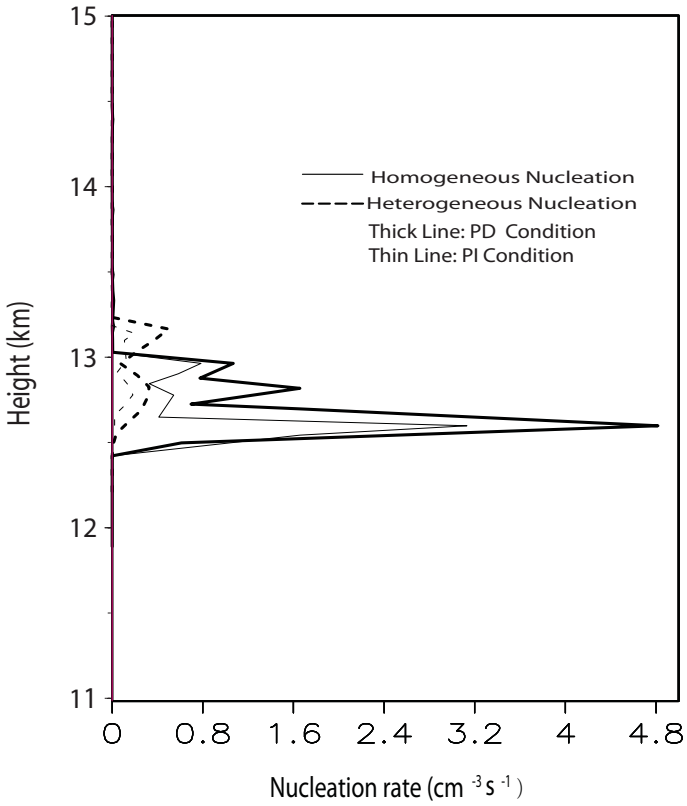

Fig. 7. Vertical distribution of the time- and area-averaged homogeneous and heterogeneous nucleation rates.

ACPD
10, 10429–10462, 2010